Supporting Information

Beyond Strain and Ligand Effects: Microstrain-Induced Enhancement of the Oxygen Reduction Reaction Kinetics on Various PtNi/C Nanostructures

Raphaël Chattot [†,‡,], Tristan Asset [†,‡], Pierre Bordet [⊥,ς], Jakub Drnec [ψ], Laetitia Dubau [†,‡] and Frédéric Maillard [†,‡,*]*

† Univ. Grenoble Alpes, LEPMI, F-38000 Grenoble, France

‡ CNRS, LEPMI, F-38000 Grenoble, France

⊥ Université Grenoble Alpes, Institut Néel, F-38000 Grenoble, France

ς CNRS, Institut Néel, F-38000 Grenoble, France

ψ European Synchrotron Radiation Facility, ID 31 Beamline, BP 220, F-38043 Grenoble Cedex, France

*To whom correspondence should be addressed. E-mail: (R.C.) raphael.chattot@grenoble-inp.org; (F.M.) frederic.maillard@lepmi.grenoble-inp.fr

This Supplementary Materials file includes:

Figures S1 to S8

Table S1 to S2

References

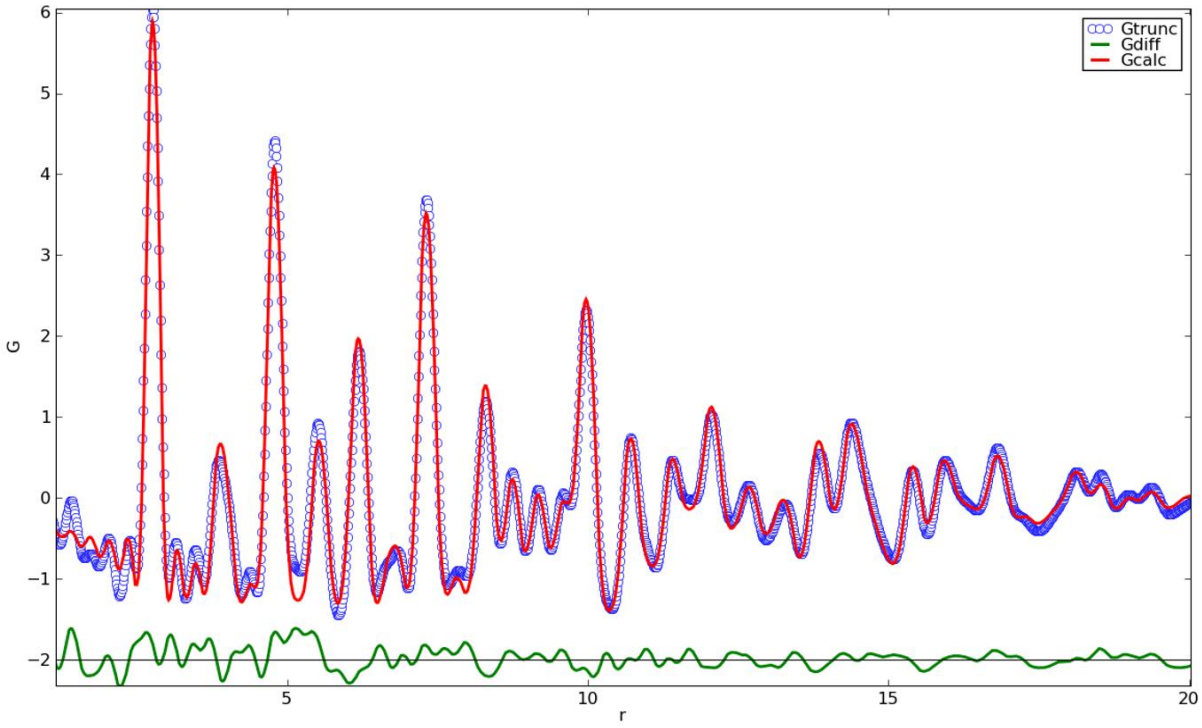

Figure S1. Plot showing the results of the PDF refinement between *r* =1 and 20 Å for the Ni@Pt/C sample. Blue circles: measured *G*(r) ($Å^{-2}$), red line: calculated *G*(r), green line: difference between experimental and calculated *G*(r). The Ni-Ni distance at *r* = 2.5 Å is not detected.

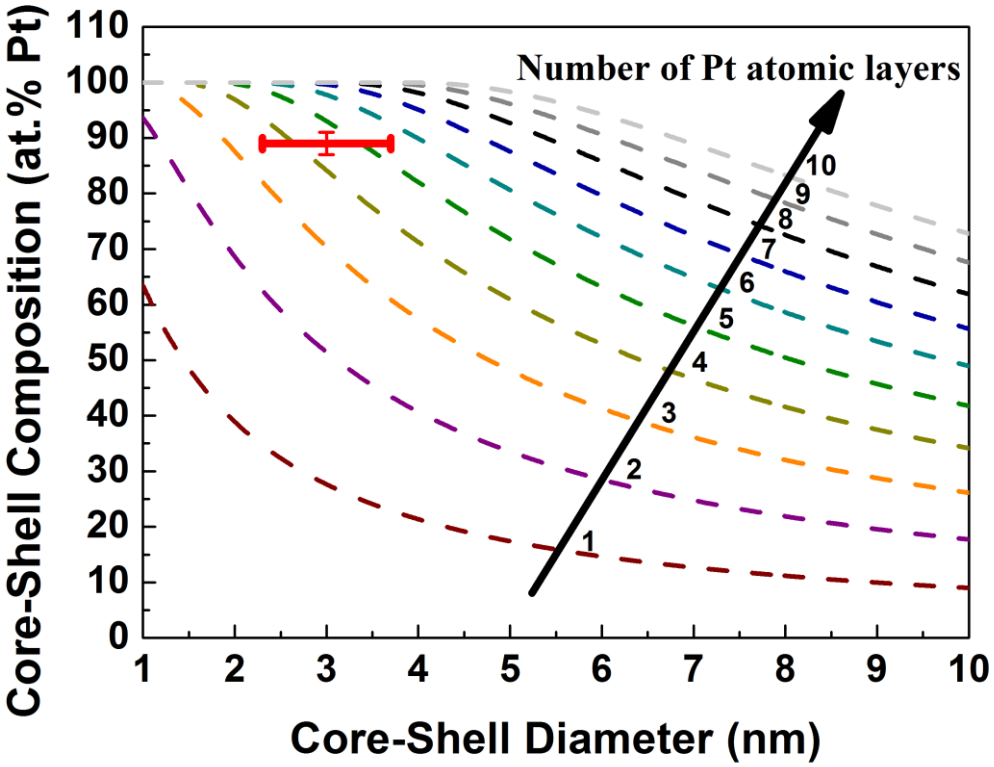

Figure S2. Relation between the chemical composition and the diameter of the core@shell nanoparticles established from the model of Montejano-Carrizales et al. [1,2]. The red symbol is the intersection of the composition of the core-shell catalyst measured by X-EDS and the particle size measured by TEM. According to the model, the Ni@Pt/C catalyst features a 4.5 ± 1 layers thick Pt shell.

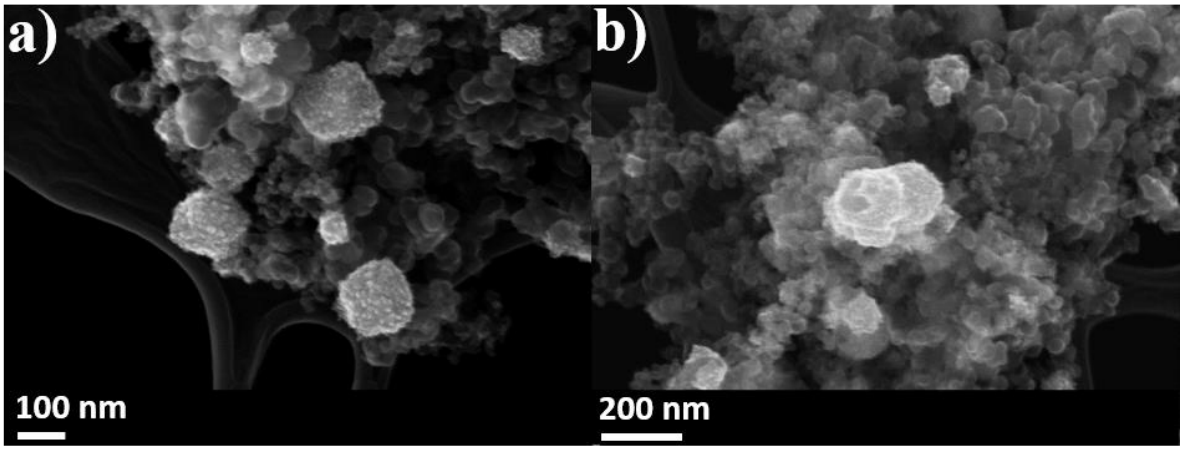

Figure S3. Scanning electron microscopy images of the "sea sponge" PtNi/C catalyst providing evidences of open porosity.

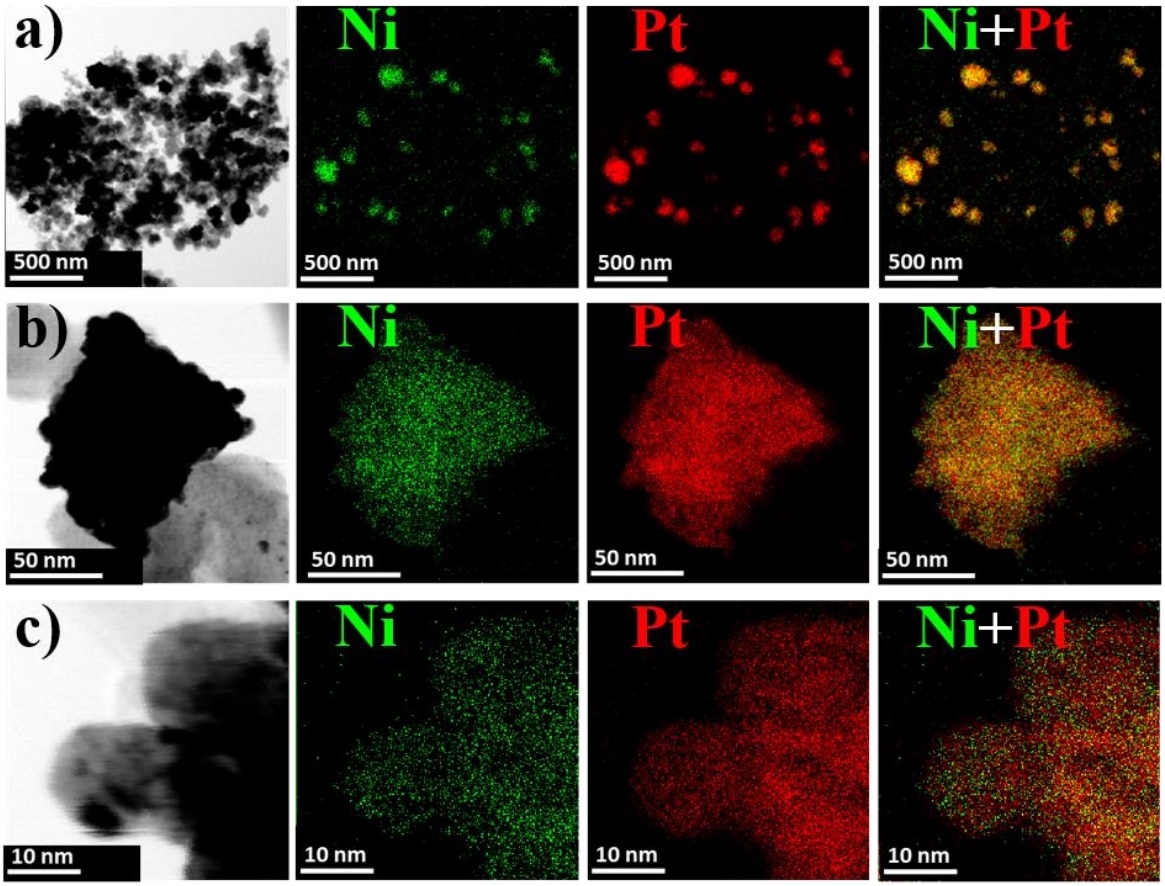

Figure S4. STEM images and X-EDS elemental maps for the "sea sponge" PtNi/C catalyst.

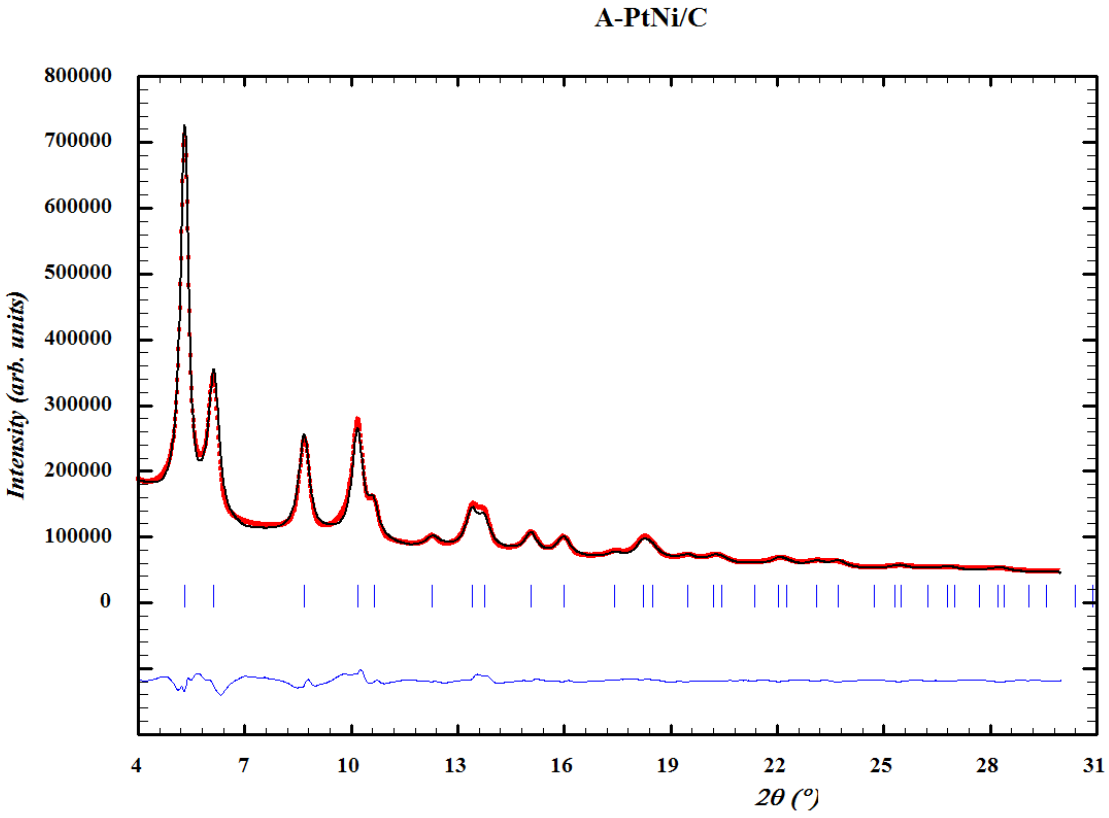

Figure S5. Plot showing the results of the Rietveld refinement of WAXS spectrum for the agglomerated PtNi/C catalyst (A-PtNi/C) synthesized in this study. Red circles: measured pattern, black line: calculated pattern, blue line: difference between measured and calculated patterns.

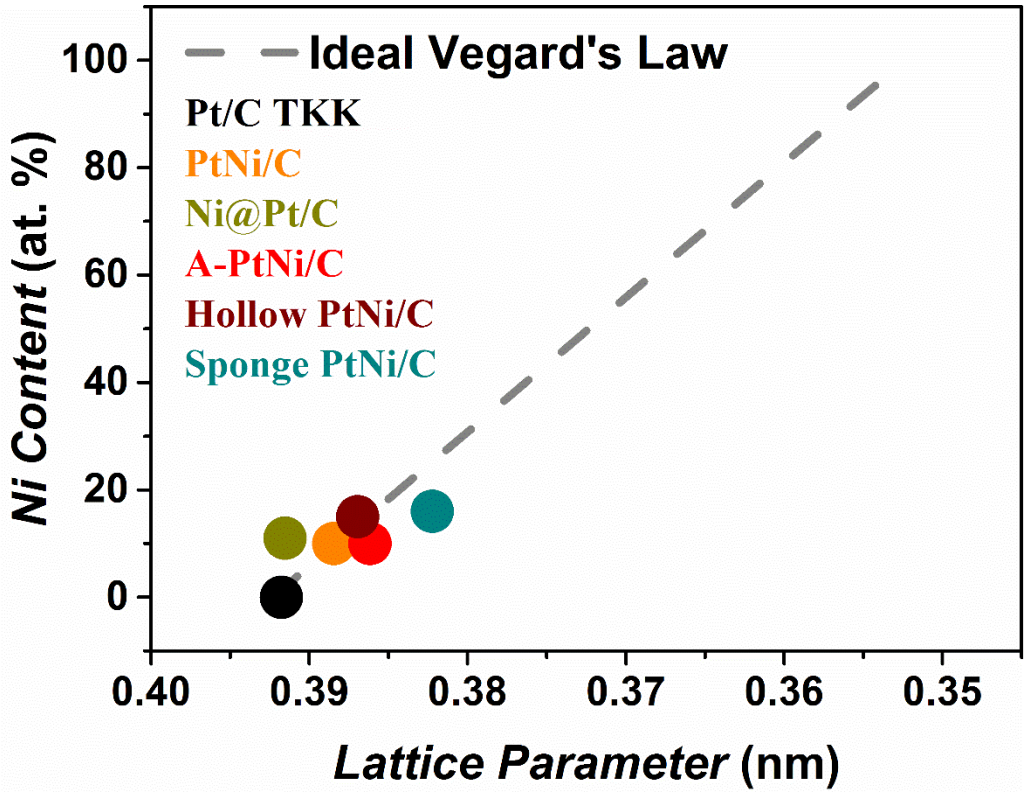

Figure S6. Ni composition measured by X-EDS *vs*. lattice parameter calculated from Rietveld refinement of the WAXS patterns for the electrocatalysts investigated in this study. The chemical composition predicted by the Vegard's law is represented as a dotted line.

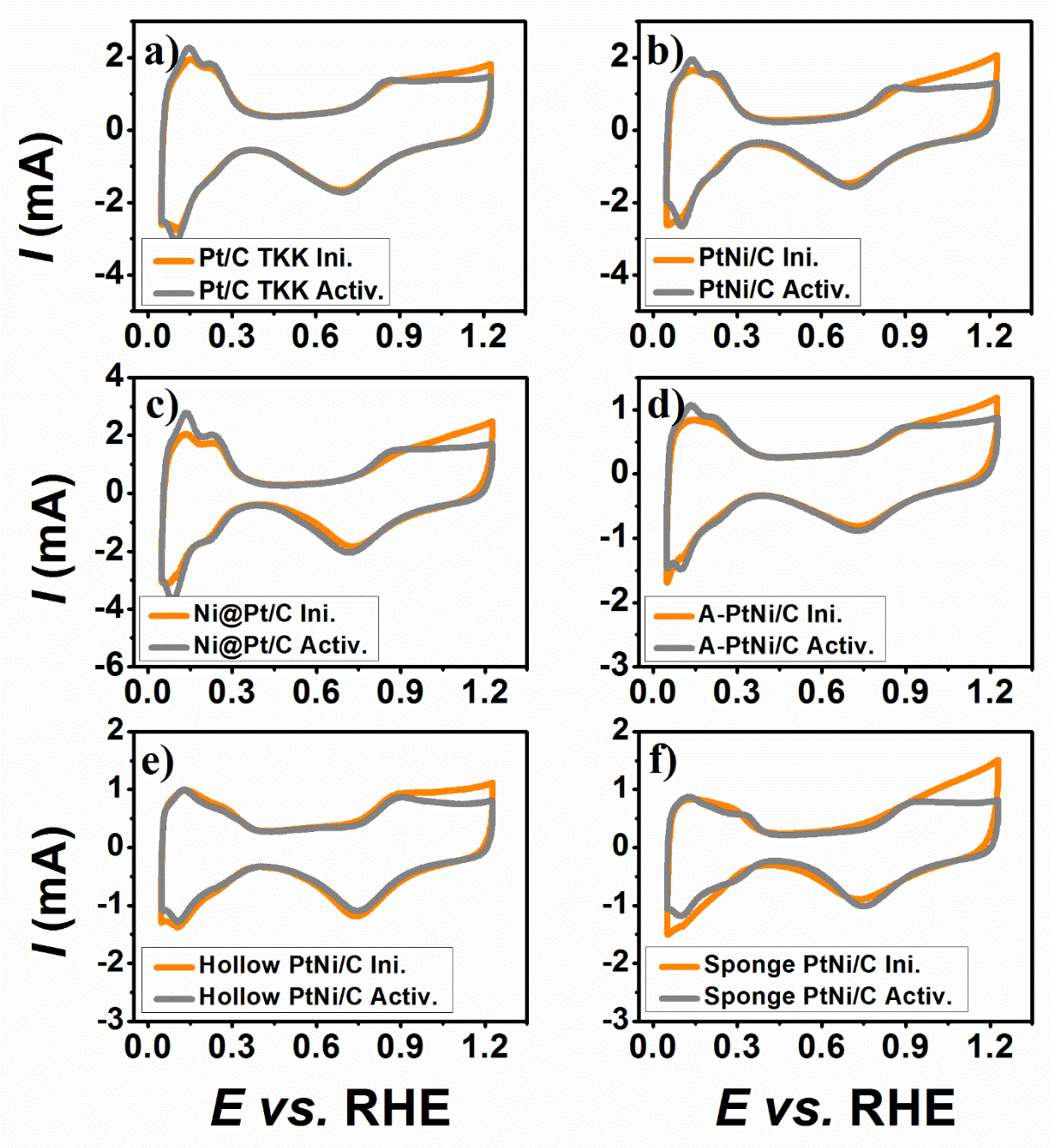

Figure S7. Cyclic voltammograms measured before (1st scan) and after (50th scan) electrochemical activation for (a) the reference Pt/C TKK, (b) PtNi/C, (c) Ni@Pt/C, (d) A-PtNi/C, (e) hollow PtNi/C, and (f) "sea-sponge" PtNi/C (f) catalysts. Ar-saturated 0.1 M $HClO_4$; v = 0.500 V s^{-1}; T = 298 ± 1 K; no rotation of the electrode; Pt loading: 3.92 µg.

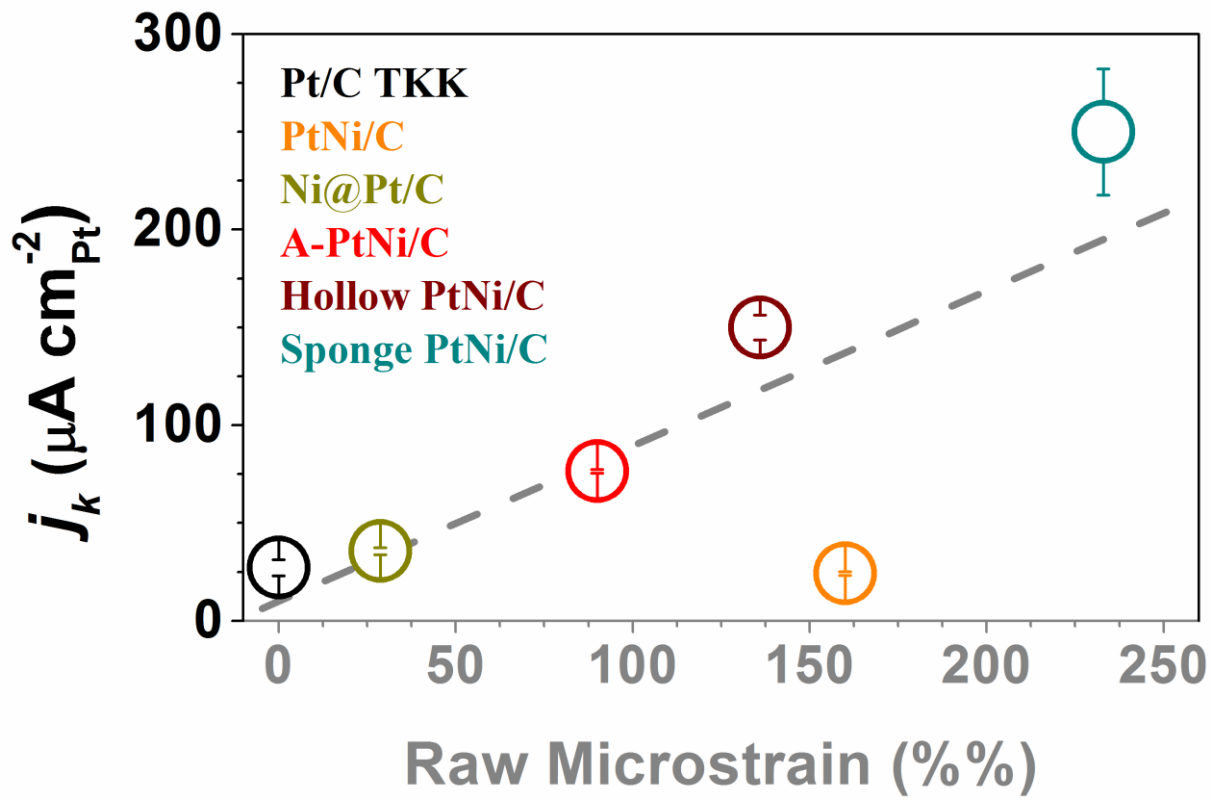

Figure S8. Relationship between the ORR specific activity measured at E = 0.95 V *vs*. RHE and the raw microstrain for the different nanostructures evaluated in this study. The raw microstrain is related to the density of structural defects, which are present in the nanocatalysts). The ORR specific activity were extracted from ORR voltammograms measured in O_2-saturated 0.1 M $HClO_4$ at a potential sweep rate v = 0.005 V s^{-1} after correction from Ohmic losses and diffusion in solution. Other conditions: T = 298 ± 1 K, Pt loading = 3.92 μg, ω = 1600 rpm.

Table S1. Structural/microstructural parameters and agreement factors obtained by Rietveld refinements of Synchrotron WAXS data for the samples investigated in this study. R_{Bragg} and R_{wp} are agreement factors for integrated intensities of the Bragg peaks and pattern profile, respectively.

	a (nm)	U_{iso} (10^{-2} nm^2)	Size (nm)	Strain (%%)	Size anisotropy (nm)	R_{wp}	R_{Bragg}
Ni@Pt/C	0.39153(2)	0.07(2)	1.79 (3)	29(7)	0.15(1)	8.05	1.91
A-PtNi/C	0.38616(2)	0.11(2)	3.9 (1)	90(5)	0.45(2)	9.57	3.05
PtNi/C	0.38845(4)	0.06(4)	1.23 (3)	160(20)	0.18(7)	6.87	1.21
Hollow PtNi/C	0.38671(2)	0.07(2)	2.69(5)	136(7)	0.36(1)	6.25	1.89
Pt/C TKK	0.39176(2)	0.45(1)	1.28(1)	0	0.15(4)	5.83	0.82
Sponge PtNi/C	0.38222(2)	0.13(2)	4.5(1)	233(7)	0.86(8)	6.55	1.22

Table S2. iR + mass transport corrected ORR specific activity ($SA_{0.90}$) and mass activity ($MA_{0.90}$) measured at E = 0.90 V *vs*. RHE on the PtNi/C nanostructures and the reference Pt/C TKK, and corresponding enhancement factor (E.F.). The ORR activity was determined in O_2-saturated 0.1 M $HClO_4$ at a potential sweep rate v = 0.005 V s^{-1}. Other conditions: T = 298 ± 1 K, Pt loading = 3.92 µg, ω = 1600 rpm.

Electrocatalyst	$SA_{0.90}$ ($\mu A\ cm_{Pt}^{-2}$)	E. F. SA	$MA_{0.90}$ ($A\ g_{Pt}^{-1}$)	E. F. MA
Pt/C TKK	229 ± 4	1	178 ± 14	1
PtNi/C	237 ± 17	1	246 ± 10	1.4
A-PtNi/C	660 ± 14	2.9	260 ± 111	1.5
Ni@Pt/C	290 ± 33	1.2	273 ± 13	1.5
Hollow PtNi/C	1444 ± 108	6.3	594 ± 95	3.3
Sea sponge PtNi/C	1733 ± 298	7.5	852 ± 219	4.8

REFERENCES

(1) Montejano-Carrizales, J. M.; Aguilera-Granja, F.; Morán-López, J. L. *Nanostructured Mater.* **1997**, *8* (3), 269–287.

(2) Montejano-Carrizales, J. M.; Morán-López, J. L. *Nanostructured Mater.* **1992**, *1* (5), 397–409.